

Article

Oxidation-Induced Changes in the Lattice Structure of YSZ Deposited by EB-PVD in High-Vacuum Conditions

Gye-Won Lee ^{1,2}, In-Hwan Lee ²  and Yoon-Suk Oh ^{1,*}

¹ Engineering Materials Center, Korea Institute of Ceramic Engineering and Technology, Icheon 17303, Republic of Korea

² Department of Materials Science and Engineering, Korea University, 145 Anam-ro, Seongbuk-gu, Seoul 02841, Republic of Korea

* Correspondence: ysoh30@kicet.re.kr

Abstract: Yttria-stabilized zirconia (YSZ), a thermal barrier coating material characterized by low thermal conductivity, is typically deposited via electron beam-physical vapor deposition. Notably, oxygen depletion occurs during this process, causing color changes in YSZ. Therefore, YSZ is speculated to undergo phase transformation during this process, which demands careful consideration owing to its effect on the life of thermal coatings. To study this phenomenon, bulk samples were prepared, subjected to vacuum heat treatment to induce oxygen depletion, and followed by oxidative heat treatment. Experimental results showed that the color of the samples changed to black after the vacuum heat treatment and to a lighter color after the oxidative heat treatment. In addition, X-ray diffraction and Raman analyses were performed. The monoclinic phase formation was confirmed during the vacuum heat treatment; however, it disappeared after the oxidation heat treatment. The coating obtained in a high vacuum atmosphere exhibited a black color and cubic phase, which changed to a bright color and tetragonal phase after the oxidation heat treatment.

Keywords: thermal barrier coating (TBC); yttria-stabilized zirconia (YSZ); EB-PVD; phase analysis



Citation: Lee, G.-W.; Lee, I.-H.; Oh, Y.-S. Oxidation-Induced Changes in the Lattice Structure of YSZ Deposited by EB-PVD in High-Vacuum Conditions. *Processes* **2023**, *11*, 2743. <https://doi.org/10.3390/pr11092743>

Academic Editor: Zhibin Lin

Received: 22 August 2023

Revised: 6 September 2023

Accepted: 9 September 2023

Published: 14 September 2023



Copyright: © 2023 by the authors. Licensee MDPI, Basel, Switzerland. This article is an open access article distributed under the terms and conditions of the Creative Commons Attribution (CC BY) license (<https://creativecommons.org/licenses/by/4.0/>).

1. Introduction

Aviation gas turbine engines are composed of various components, such as compressors, turbines, and combustion chambers, which are repeatedly exposed to high-temperature combustion environments and room-temperature environments. To withstand such thermal loads, gas turbine components are typically composed of Ni-based superalloys, known for their excellent properties such as high temperature resistance and oxidation resistance [1–4]. The operating limit temperature of the superalloy materials used in gas turbine engines is known to be 900–1050 °C. With growing demands for the improved efficiency of gas turbine engines, considerable research efforts have been devoted to increase the engine operating temperature and reduce the weight of gas turbine parts. By applying thermal barrier coatings (TBCs) to the surface of Ni-based superalloy materials, the operating temperature of gas turbines can be increased [1–9]. In particular, TBCs inhibit the transfer of heat generated during gas turbine operation to the surface of the superalloy, thereby improving the life and operating temperature of gas turbine components. A TBC typically consists of a ceramic top coat, characterized by low thermal conductivity and excellent oxidation resistance, and a bond coat with excellent adhesion and oxidation resistance, located between the top coat and the substrate [7–10]. TBC's bond coat is typically made of MCrAlY (M = Ni, Co, or a mixture of both compositions) or a β -NiAl diffused aluminide layer. Aviation gas turbine engines typically use an aluminide layer as a bond coat. Although the aluminide layer functions to prevent oxygen penetration to the surface of the Ni-based superalloy material in high temperature operating environments, it reacts with the oxygen penetrating the top coat and forms a thermally grown oxide (TGO) layer. This TGO layer usually consists of Al_2O_3 formed by the reaction of aluminum (Al) and oxygen

(O₂) in the bond coat layer. Furthermore, this TGO layer is known to cause delamination of the top coat. To address this problem, research is being actively conducted on composite aluminide bond coats with Pt, Hf, and so on added to the aluminide layer [11–16].

Zirconia, which has a high coefficient of thermal expansion, low thermal conductivity, and excellent fracture toughness, is a promising top coat material for TBCs. Moreover, zirconia exhibits three phases and undergoes temperature-dependent phase transformation: monoclinic phase from 25 °C to 1173 °C, tetragonal phase from 1173 °C to 2370 °C, and cubic phase at higher temperatures. Notably, a volume change of approximately 3–5% occurs during transformation between monoclinic and tetragonal phases, which induces stress on the top coat, resulting in decreased longevity of the coating. A promising strategy to suppress this phase transformation is to dope zirconia with trivalent or quaternary oxides. Among these frameworks, a notable one is yttria (Y₂O₃)-stabilized zirconia (YSZ), obtained by doping 6–8 wt% of yttria on zirconia. In addition to stabilizing zirconia in the tetragonal phase at room temperature, yttria serves to reduce the thermal conductivity by forming oxygen vacancies inside the lattice structure of zirconia [17–20]. The main strategies for introducing YSZ materials into gas turbine components include atmospheric plasma spray (APS) and electron beam-physical vapor deposition (EB-PVD) techniques. YSZ coatings prepared using these methods have a non-transformable tetragonal phase (t'). In this t' configuration, the tetragonal phase does not transform to a monoclinic phase even when exposed to cyclic temperature variations between high and room temperatures [21–23].

When these YSZs are exposed to temperatures above 1200 °C for a long time, phase decomposition of the tetragonal phase occurs to form monoclinic and cubic phases. In addition, the operating temperature of gas turbine engines is continuously increasing, and various materials are being studied to address this situation (see Table 1). Rare earth-doped zirconia, which adds various rare earths in addition to yttria to zirconia, can reduce thermal conductivity by causing lattice distortion inside zirconia lattice structures. However, when large amounts of rare earths are added, some of the tetragonal phase of zirconia may transform to a cubic phase. This phase transformation can cause a decrease in the cyclic lifetime of the coating layer, which can lead to a decrease in the durability of the coating layer. Perovskites such as SrZrO₃ have features suitable for TBC, such as a high coefficient of thermal expansion and lower thermal conductivity than that of YSZ. Hexaaluminates, also called lanthanum hexaaluminates, have thermal conductivities similar to those of YSZ. They have high sintering resistances and structural stabilities at temperatures above 1400 °C. Pyrochlores are characterized by low thermal conductivities, high temperature phase stabilities, and CMAS (Calcium-Magnesium-Aluminum-Silicon Oxide) resistances. Various zirconia-based materials are being actively researched to improve the performance of YSZ [24].

Table 1. New Materials for Thermal Barrier Coating Ceramic Top Coat.

Material Group	Example
RE-doped ZrO ₂	Nd ₂ O ₃ -Yb ₂ O ₃ -Y ₂ O ₃ -ZrO ₂ Yb ₂ O ₃ -Gd ₂ O ₃ -Y ₂ O ₃ -ZrO ₂
Perovskites	BaZrO ₃ SrZrO ₃ CaZrO ₃
Hexa-aluminates	LaMgAl ₁₁ O ₁₉ GdMgAl ₁₁ O ₁₉
Pyrochlores	La ₂ Zr ₂ O ₇ Nd ₂ Zr ₂ O ₇ Sm ₂ Zr ₂ O ₇ Eu ₂ Zr ₂ O ₇ Gd ₂ Zr ₂ O ₇

The top coats produced by APS are commonly used in power generation gas turbines, whereas the EB-PVD method is mainly applied to aviation gas turbines. When the EB-PVD is used, the resulting coating layer has a columnar structure with gaps between the columns, leading to a higher thermal conductivity than those of APS-manufactured coatings. However, EB-PVD-derived layers exhibit excellent mechanical properties such as adhesion and are thus preferred for aviation gas turbine parts [25–29]. Notably, the EB-PVD process requires a high-vacuum environment for YSZ deposition, and the YSZ is evaporated by an electron beam in such conditions [28,29]. During evaporation, part of the oxygen in the YSZ lattice structure is dissolved. To compensate for this oxygen loss, supplementary oxygen is introduced [30]. However, if an inadequate amount of oxygen is supplied, the color of the YSZ coating darkens. Previous studies have mainly focused on analyzing the properties of monolithic YSZ or monolithic modified zirconia. Therefore, it is necessary to consider the changes in the properties of YSZ coatings caused by the high vacuum atmosphere during the EB-PVD process [31,32].

Considering these aspects, in this study, bulk samples and EB-PVD coating samples were prepared to compare the changes in the crystal structure of YSZ deposited in vacuum conditions with those of corresponding coatings subjected to oxidation heat treatment. To investigate the property change behavior of YSZ, the bulk samples were subjected to vacuum heat treatment to eliminate oxygen in the YSZ crystal structure. Subsequently, the bulk samples were oxidized in an electric furnace via an oxidation heat treatment to study the effect of the reintroduction of oxygen into the crystal structure of YSZ which changed by vacuum heat treatment. XRD and Raman spectroscopy analyses were performed before and after the heat treatment of the bulk sample to compare the phase change behaviors based on oxygen in the crystal structure.

Furthermore, YSZ samples were deposited via the EB-PVD technique without oxygen in a high-vacuum atmosphere to confirm the physical properties of the YSZ coatings, and the coatings were subjected to oxidation heat treatment in an electric furnace after phase analysis. Same as the bulk sample, XRD and Raman Spectroscopy were performed before and after the oxidation heat treatment of the coating sample to compare the phase formation behaviors based on oxygen in the crystal structure.

2. Materials and Methods

2.1. Sample Preparation

To prepare YSZ coating samples in high-vacuum conditions, a 7 wt% YSZ ingot (Saint-Gobain, France) with a diameter of 60 mm and a thickness of 150 mm was deposited on an Inconel 718-3 substrate without substrate rotation using EB-PVD (KICET, Icheon, Republic of Korea) equipment. The deposition was performed in a high-vacuum environment with a pressure of 10^{-6} torr, using a beam power of 20 kW for 1 h. Moreover, an 8 wt% YSZ (Hankyung TEC, Jinju, Republic of Korea) powder with an average particle size of 1 μm was used, and granulated powder was obtained by spray drying at an inlet temperature of 165 $^{\circ}\text{C}$, outlet temperature of 70 $^{\circ}\text{C}$, and atomizer speed of 9500 rpm. The granulated powder was densified by sintering heat treatment at 1200 $^{\circ}\text{C}$ for 4 h. To produce bulk samples to be exposed to a low vacuum environment, the sintered powders were mixed with YSZ powder with an average particle size of 1 μm , and samples with a diameter of 55 mm and thickness of 50 mm were molded by uniaxial pressing. The uniaxial pressurized bulk samples were subjected to vacuum heat treatment at 1400 $^{\circ}\text{C}$ for 10 h in a vacuum furnace (Ajeon Heating Industry, Namyangju, Republic of Korea) with a vacuum level of 10^{-3} torr. To restore the lattice structure through oxidation of the bulk and coating samples produced in each condition, the samples were subjected to oxidation heat treatment in an electric furnace at 1000 $^{\circ}\text{C}$ for 50 h under atmospheric pressure conditions.

2.2. Characterization

After the vacuum heat treatment of the bulk sample, chromaticity analysis was performed on portions exposed to the vacuum atmosphere using a spectrophotometer (Cm-

700d, Konica Minolta, Chiyoda, Japan). Among the CIE $L^* a^* b^*$ values obtained through this analysis, the L^* value, which can distinguish white and black, was examined. An L^* value closer to 100 and 0 represents a color closer to white and black, respectively. XRD (RINT-2500HF, Rigaku, Tokyo, Japan) analysis was performed to investigate the pre- and post-oxidation phases of the YSZ produced in each vacuum condition. To distinguish the monoclinic phase of zirconia from the tetragonal and cubic phases, the $10\text{--}80^\circ$ region was scanned at settings of 40 kV, 100 mA, and $5^\circ/\text{min}$. To distinguish between the tetragonal and cubic phases of zirconia, the $72\text{--}76^\circ$ region was scanned at a speed of $0.2^\circ/\text{min}$ to confirm the phase formation. To improve the accuracy of the XRD-based zirconia phase analysis, Raman spectroscopy (Invia Raman Microscope, Renishaw, New Mills, UK) was performed to validate the phase of zirconia in a vacuum environment and its phase following oxidation. An Ar laser (514 nm) was used for the analysis, and the scan range was set to be from 100 to 700 cm^{-1} .

3. Results

Figure 1 shows the XRD results of the 8 wt% YSZ bulk sample before vacuum heat treatment. The monoclinic phase was not observed when scanning the $10\text{--}80^\circ$ region. When scanning the $72\text{--}76^\circ$ region, only the tetragonal phase was detected, and the cubic phase was absent.

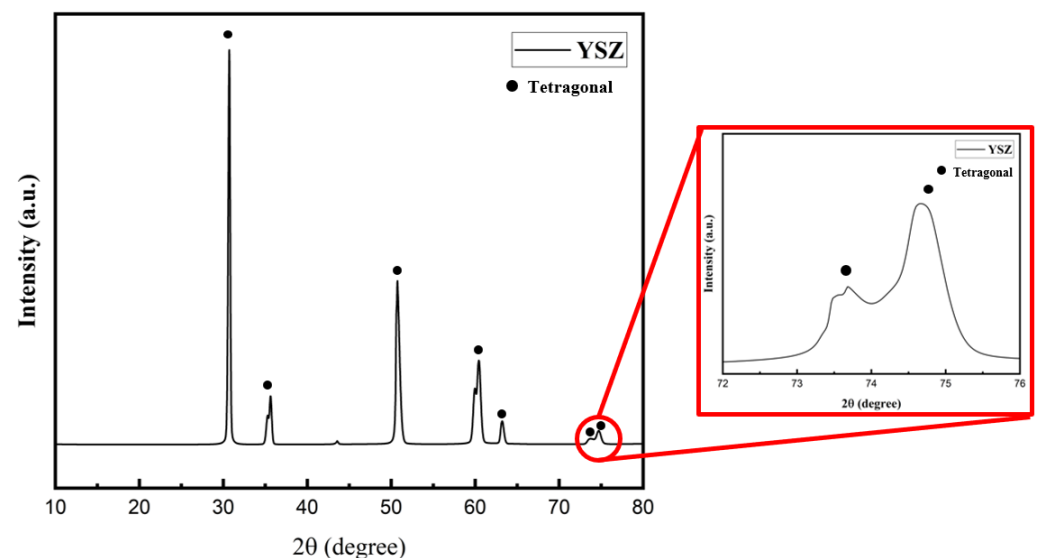


Figure 1. Before Vacuum Heat Treatment 8 wt% YSZ Bulk Sample XRD Result.

In the assessment of the sample color following vacuum annealing, different surface areas exposed to the low vacuum atmosphere displayed varying shades, as depicted in Figure 2. Regions exposed to low vacuum and high temperature conditions were darker in color, whereas the areas less influenced by the atmosphere demonstrated a milder color shift.

The results of the color analysis based on the spectrophotometer are summarized in Table 2. The average L^* value for the upper section of the sample, which was more exposed to the vacuum environment, was 39.5., and the average L^* value for the lower section of the sample, which was less exposed to the vacuum environment, was 64.93. The difference in color was attributable to the difference in the effect of the vacuum environment. The oxygen present in the zirconia lattice structure escaped and formed additional vacancies in the crystal structure, thereby affecting the wavelength of light absorbed within the crystal structure. Consequently, the color shifted from white to a darker hue [32–34]. In particular, areas more profoundly affected by the vacuum environment assumed darker hues owing to oxygen scarcity, whereas less influenced regions appeared lighter owing to the higher oxygen concentration within the lattice structure.

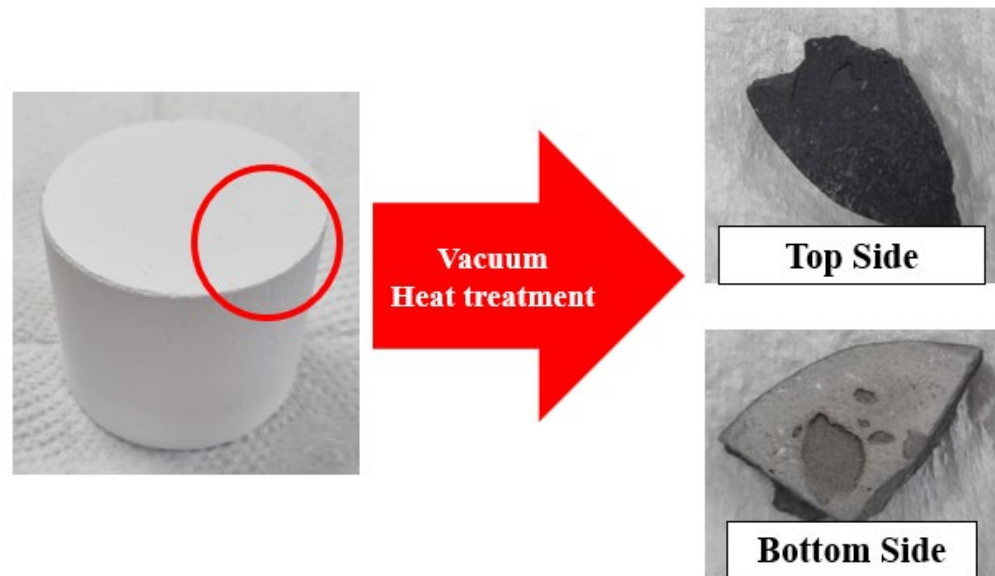


Figure 2. 8 wt% YSZ Bulk Sample Image. (Sample gained from red circl).

Table 2. After Vacuum Heat Treatment 8 wt% YSZ Bulk Sample Spectrophotometer.

L* Result Number	Sample Top Surface	Sample Bottom Surface
1	40.72	64.5
2	39.16	64.93
3	38.62	65.36
Average	39.5	64.93

Figure 3 shows the XRD spectra of the YSZ sample subjected to vacuum heat treatment. The 10–80° scan revealed the formation of the monoclinic phase, whereas the 72–76° scan indicated a mixture of tetragonal and cubic phases. The formation of monoclinic and cubic phases in the sample after vacuum heat treatment can be explained as follows: The oxygen present in the lattice structure escaped during vacuum heat treatment, thereby forming vacancies inside the lattice structure. These vacancies affected the size of the lattice structure of zirconia, leading to the transformation of the tetragonal phase into monoclinic and cubic phases [32].

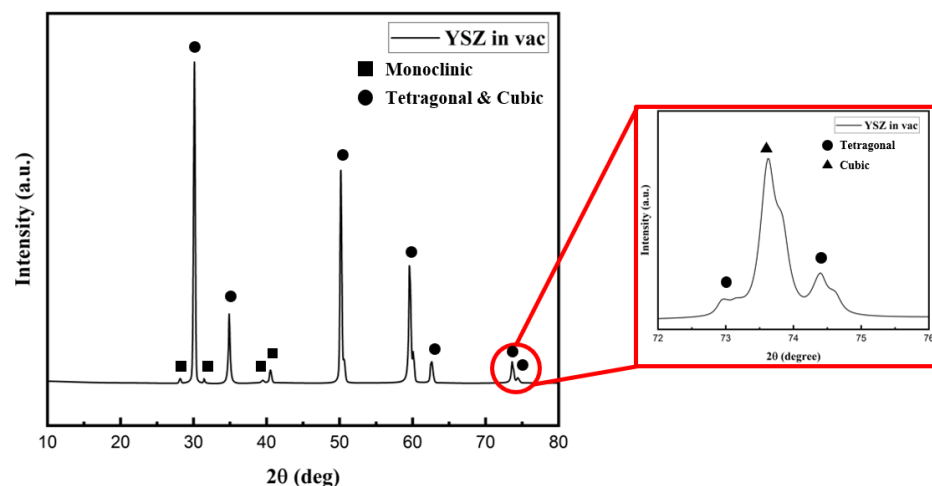


Figure 3. After Vacuum heat Treatment 8 wt% YSZ Bulk Sample XRD Result.

Figure 4 shows the XRD results of the vacuum annealed bulk sample subjected to oxidation annealing at 1000 °C for 50 h. In the 10–80° regime, no monoclinic phase was

detected. This result indicated that the tetragonal phase transformed to the monoclinic phase owing to the increased oxygen vacancies caused by the loss of oxygen in the lattice structure. However, these oxygen vacancies were reoccupied through the oxidation heat treatment, resulting in the disappearance of the monoclinic phase. In the 72–76° regime, the bulk sample subjected to oxidation heat treatment exhibited tetragonal and cubic phases. These results demonstrated that although the change in the lattice structure induced by vacuum heat treatment could be rectified by oxidation heat treatment, the cubic phase (with a crystal structure similar to that of the tetragonal phase) could not be transformed to the tetragonal phase.

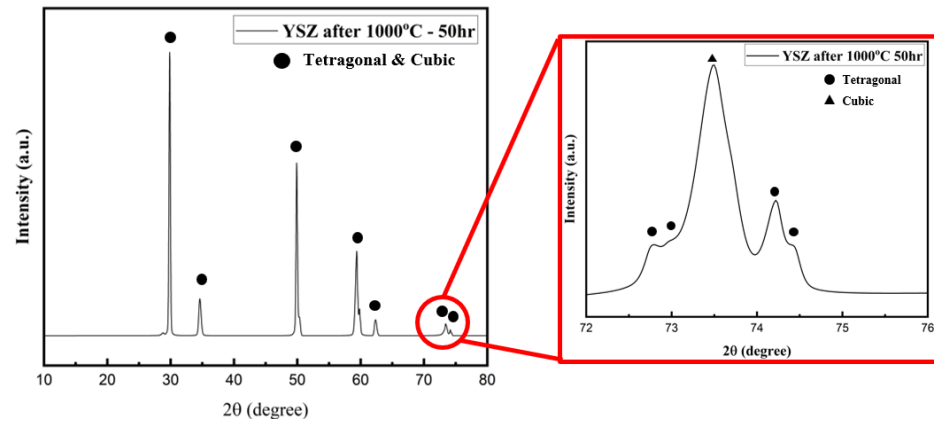


Figure 4. After Heat Treatment 1000 °C-50 h 8 wt% YSZ Bulk Sample XRD Result.

Raman spectrum analysis provided further insights into the YSZ phase characteristics. Peaks corresponding to the monoclinic phase were detected at 183, 301, 335, 381, 476, 536, 559, 613, and 636 cm^{-1} , with the peaks at 183, 335, and 476 cm^{-1} appearing prominent. Peaks corresponding to the tetragonal phase were observed at 149, 224, 292, 324, 407, 456, and 636 cm^{-1} . The peaks for the cubic phase were similar to those of the tetragonal phase; however, the peak at 636 cm^{-1} was replaced by that at 628 cm^{-1} . Figure 5 shows the Raman spectra after vacuum annealing and oxidation annealing of the bulk sample.

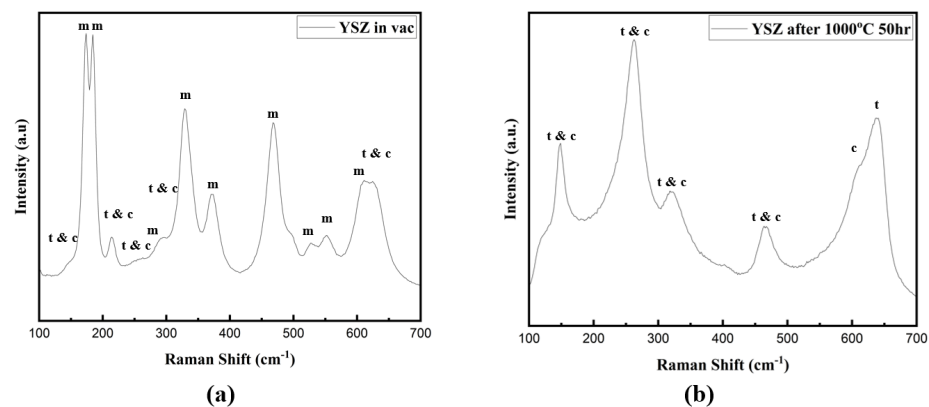


Figure 5. 8 wt% YSZ Bulk Sample Raman Spectroscopy Result. (a) after Vacuum heat treatment (b) after Oxidation at 1000 °C-50 h.

As shown in Figure 5a, peaks corresponding to the monoclinic, tetragonal, and cubic phases appeared at 145, 181, 217, 294, 332, 375, 470, 528, 553, 611, and 626 cm^{-1} . A comparison of the peak positions indicated that the tetragonal phase transformed into the monoclinic and cubic phases owing to the oxygen loss during vacuum heat treatment. Figure 5b shows the Raman spectra after oxidation heat treatment. Peaks at 148, 262, 323, 466, and 637 cm^{-1} , along with a shoulder peak at 614 cm^{-1} , could be identified. The

shoulder peak indicated the presence of the cubic phase, suggesting the coexistence of the tetragonal and cubic phases. Notably, in the zirconia lattice structure, the oxygen vacancies that were lost during vacuum heat treatment were reoccupied through oxidation heat treatment. Thus, the lattice structure was altered again; however, the cubic phase was formed with the restoration of the tetragonal phase. This result could be attributable to the similarity in the crystal structures of the tetragonal and cubic phases. When the oxygen in the zirconia lattice structure escapes during vacuum heat treatment, the c-axis of the lattice structure is modified, resulting in a phase change from tetragonal to cubic. This phase change indicates that it is difficult to restore the initial tetragonal phase of zirconia even if the lattice structure is refilled with oxygen by oxidation heat treatment.

The phenomenon of color change in the bulk sample was also observed in the EB-PVD coating sample. Figure 6 shows the EB-PVD coating sample (a) post deposition in vacuum conditions and (b) after oxidation heat treatment. In Figure 6a, oxygen depletion occurred in the YSZ lattice structure during the EB-PVD process. Probably, these depletions were deposited with unfilled defects, which resulted in the darker color of the coating layer. In Figure 6b, probably the oxygen vacancies in the lattice structure of YSZ that occurred during the high-vacuum deposition process were filled with oxygen during the oxidation heat treatment. The color of the coating sample changed to a lighter color.

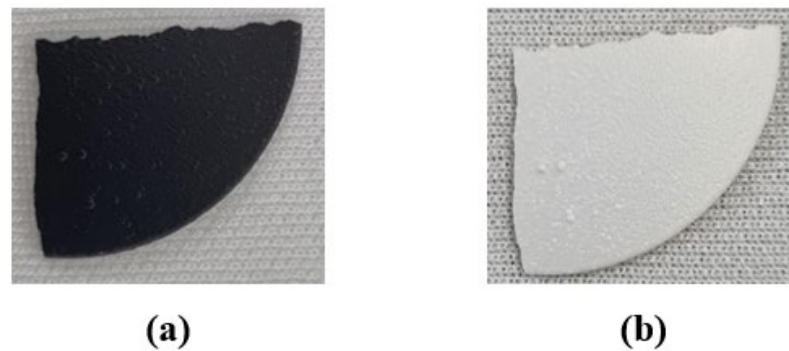


Figure 6. YSZ EB-PVD Coating Sample Image (a) after coating (b) after 1000 °C-50 h heat treatment.

Figure 7 shows the XRD results of the samples deposited in a high-vacuum atmosphere. The monoclinic phase was not identified in the 10–80° scan (Figure 7a). In the 72–76° regime (Figure 7b), only the cubic peak was observed. In both cases, the peaks were broad. Notably, 7 wt% YSZ deposited by EB-PVD typically exhibits a tetragonal phase. However, only the cubic phase was identified in the XRD analysis. This difference may be attributable to the oxygen depletion caused by the high-vacuum environment during coating, resulting in the emergence of numerous lattice defects and changes in the lattice structure.

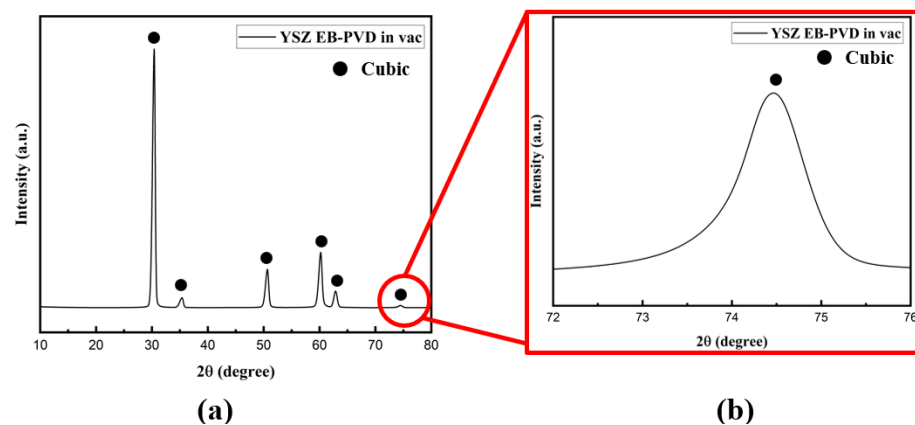


Figure 7. YSZ Coating Sample XRD Result After EB-PVD Coating. (a) XRD results of 10–80° scan (b) XRD results of 72–76° scan.

The XRD results of the vacuum-annealed samples subjected to the oxidation heat treatment are depicted in Figure 8. Following the oxidation heat treatment, no monoclinic phase was formed; however, the tetragonal phase was detected. In addition, the broad peak seen in the XRD analysis of the high-vacuum deposition sample changed to a sharp shape as the crystal structure changed through the oxidation heat treatment, and a tetragonal peak was identified in the 72–76° region.

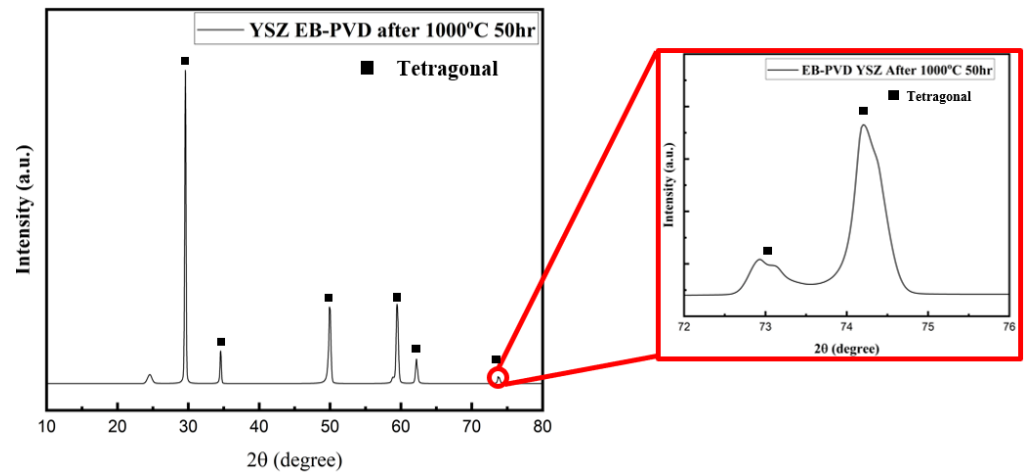


Figure 8. YSZ Coating Sample XRD Result at 1000 °C-50 h heat treatment.

Figure 9a shows the Raman spectra of the sample subjected to EB-PVD in high-vacuum conditions. No monoclinic peak was identified, and only a single peak at 635 cm^{-1} was observed. The Raman spectra of the coating sample subjected to oxidation heat treatment (Figure 9b) did not exhibit any monoclinic peak. A peak at 636 cm^{-1} was observed, indicating the presence of the tetragonal phase.

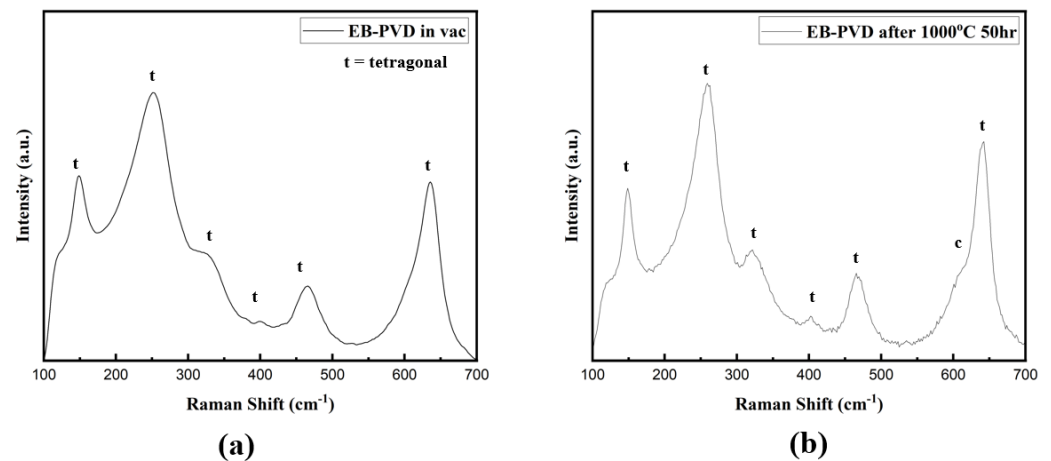


Figure 9. YSZ Coating Raman Spectroscopy Result. (a) After Coating (b) After 1000 °C–50 h heat treatment.

Overall, YSZ deposited through EB-PVD in a high-vacuum condition without oxygen exhibited a cubic phase according to the XRD results and a tetragonal phase according to Raman spectra. Together, these findings suggest the presence of a near-cubic tetragonal phase, which is similar to a non-transformable tetragonal phase (t' -phase), given its tetragonality. In general, cubic and t' phases are difficult to distinguish owing to their similar crystal structures. However, a key distinction lies in the length of the c-axis within the crystal structure: Specifically, in the cubic phase, all three axes (a , b , and c) have the same lengths. In contrast, in the tetragonal phase, the c-axis is elongated while the a

and b axes have the same length. The length of the c-axis in the t' -phase is shorter than that in the tetragonal phase [17,35]. The deposition of the t' -phase can be explained as follows: During the deposition of YSZ in high-vacuum conditions, oxygen escapes from the lattice structure, and the resulting oxygen vacancies formed in the crystal structure shorten the c-axis of the tetragonal phase [32]. After oxidation heat treatment of the high-vacuum-deposited YSZ coating sample, only the tetragonal phase was observed without the monoclinic phase in both the XRD and Raman analyses. This observation highlights that oxidation heat treatment of YSZ deposited in high-vacuum conditions can facilitate the achievement of the tetragonal phase of YSZ without the emergence of the monoclinic phase.

4. Discussion

The vacuum heat treatment of YSZ (yttria-stabilized zirconia) bulk samples leads to a noticeable change in their color, sparking scientific curiosity. This intriguing phenomenon can be attributed to the depletion of oxygen from the YSZ crystal structure during the vacuum heat treatment process. This alteration in the crystal's oxygen content affects the optical properties of the material, resulting in a shift in the way it refracts light. Consequently, the surface color of the bulk sample transitions from its initial white appearance to a darker shade. Furthermore, the loss of oxygen from the crystal lattice during the vacuum heat treatment results in the creation of oxygen vacancies within the material. These vacancies, in turn, cause structural changes in the lattice. These changes have been substantiated through phase analyses. Notably, these analyses revealed the presence of monoclinic and cubic phases in addition to the initial tetragonal phase. To investigate the impact of oxygen depletion on the crystal structure, oxidation heat treatment was performed. This treatment revealed intriguing findings: only the monoclinic phase disappeared, leaving the cubic phase unaffected. This suggests that the cubic phase, which shares some similarities in crystal structure with the tetragonal phase, resists transformation into the tetragonal phase under the oxidation heat treatment. In contrast, the monoclinic phase, which exhibits significant differences in crystal structure from both the tetragonal and cubic phases, appears to be more amenable to transformation into either the tetragonal or cubic phase through the heat treatment. Applying these intriguing observations to coating samples obtained through electron beam physical vapor deposition (EB-PVD), it was initially hypothesized that YSZ formed in the cubic phase during vacuum deposition might not entirely convert into the tetragonal phase subsequent to the oxidation heat treatment. However, experimental results contradicted this expectation, as the cubic phase disappeared after oxidation, leaving only the tetragonal phase intact. This discrepancy in results between the bulk and coated samples suggests the potential formation of a non-transformable tetragonal phase (t' phase), one closely resembling the cubic phase, within the crystal structure of the coated sample deposited in a vacuum environment. Furthermore, considering prior research on the correlation between phases and mechanical properties of zirconia, we speculate that the tetragonal phase will be more pronounced following the oxidative heat treatment [20,25]. Consequently, we expect improved mechanical properties in the coating sample after the oxidative heat treatment compared with its state after high vacuum deposition. This expectation is based on the fracture toughness variation of YSZ with the phase of zirconia, and it is known that tetragonal-phase zirconia has higher fracture toughness than cubic-phase zirconia [24,25]. However, further experiments are required to validate these expectations.

5. Conclusions

Electron beam-physical vapor deposition (EB-PVD) is a deposition process widely used in the manufacturing of various materials, including yttria-stabilized zirconia (YSZ). When YSZ is deposited using EB-PVD in a high-vacuum environment without oxygen injection, an intriguing phenomenon occurs: the material color darkens. This change in

color is indicative of underlying transformations in its physical properties, prompting the need for a closer examination.

- Upon conducting a thorough analysis of the bulk YSZ sample before and after the vacuum heat treatment, distinct differences emerged. Initially, only the tetragonal phase was identified in the untreated sample. However, after subjecting it to a vacuum heat treatment, the sample exhibited the presence of not only a tetragonal phase but also monoclinic and cubic phases. Notably, variations in color were observed in various areas of the sample, with those highly influenced by the vacuum heat treatment atmosphere appearing darker (average L^* of 64.93) and those less affected appearing relatively lighter (average L^* of 39.5). Subsequently, through the oxidation heat treatment, the color of the bulk YSZ sample was restored to a light white hue. This treatment also led to the disappearance of the monoclinic phase of zirconia, indicating a transformation back to the original state. However, it is worth noting that the cubic phase formed during the vacuum heat treatment did not completely revert to the tetragonal phase.
- Intriguingly, X-ray diffraction (XRD) analyses performed in the $72\text{--}76^\circ$ range on the YSZ samples produced by EB-PVD in the high vacuum environment detected only the cubic phase. Conversely, Raman analysis confirmed the presence of the tetragonal phase, suggesting that the crystal structure of the YSZ sample deposited in this high vacuum atmosphere is in the t' phase. Subsequent XRD and Raman analyses of EB-PVD samples after the oxidation heat treatment indicated the existence of only the tetragonal phase. This intriguingly suggests that even if the crystal structure of YSZ undergoes changes due to deposition in a high vacuum environment, it can be restored to its original phase through oxidation heat treatment.

These findings suggest that the crystal structure of the YSZ coating undergoes changes based on the environmental conditions during the deposition process. Furthermore, it has been demonstrated that the oxidative heat treatment can effectively restore the YSZ crystal structure to closely resemble its initial state. In our future research, we intend to delve deeper into the analysis of the crystal structure of YSZ deposited in a high vacuum atmosphere and explore the effects of oxidative annealing on YSZ. Additionally, we plan to investigate the thermal and mechanical properties of these materials.

Author Contributions: Conceptualization, methodology, formal analysis, and writing—original draft, G.-W.L. and Y.-S.O.; data curation, G.-W.L.; review and editing, I.-H.L. and Y.-S.O.; project administration, Y.-S.O. All authors have read and agreed to the published version of the manuscript.

Funding: This research was supported by the Institute of Civil Military Technology Cooperation, Civil-Military Technology Development (20-CM-CE-14).

Data Availability Statement: Not applicable.

Conflicts of Interest: The authors declare no conflict of interest.

References

1. Miller, R.A. Thermal barrier coatings for aircraft engines: History and directions. *J. Therm. Spray Technol.* **1997**, *6*, 35–42. [[CrossRef](#)]
2. Xu, L.; Bo, S.; Hongde, Y.; Lei, W. Evolution of Rolls-Royce air-cooled turbine blades and feature analysis. *Procedia Eng.* **2015**, *99*, 1482–1491. [[CrossRef](#)]
3. Younossi, O.; Arena, M.V.; Moore, R.M.; Lorell, M.; Mason, J.; Graser, J.C. *Military Jet Engine Acquisition: Technology Basics and Cost-Estimating Methodology*; Rand: Santa Monica, CA, USA, 2002.
4. Toriz, F.C.; Thakker, A.B.; Gupta, S.K. Flight service evaluation of thermal barrier coatings by physical vapor deposition at 5200 H. *Surf. Coat. Technol.* **1989**, *39–40*, 161–172. [[CrossRef](#)]
5. Rigney, D.V.; Viguie, R.; Wortman, D.J.; Skelly, D.W. PVD thermal barrier coating applications and process development for aircraft engines. *J. Therm. Spray Technol.* **1997**, *6*, 167–175. [[CrossRef](#)]
6. Bobzin, K.; Bagcivan, N.; Brögelmann, T.; Yildirim, B. Influence of temperature on phase stability and thermal conductivity of single- and double-ceramic-layer EB-PVD TBC top coats consisting of 7YSZ, $Gd_2Zr_2O_7$ and $La_2Zr_2O_7$. *Surf. Coat. Technol.* **2013**, *237*, 56–64. [[CrossRef](#)]

7. Feuerstein, A.; Knapp, J.; Taylor, T.; Ashary, A.; Bolcavage, A.; Hitchman, N. Technical and economical aspects of current thermal barrier coating systems for gas turbine engines by thermal spray and EBPVD: A review. *J. Therm. Spray Technol.* **2008**, *17*, 199–213. [[CrossRef](#)]
8. Xu, Z.; Wang, Z.; Huang, G.; Mu, R.; He, L. Thermal cycling behavior of EB-PVD TBCs on CVD platinum modified aluminide coatings. *J. Alloys Compd.* **2015**, *637*, 226–233. [[CrossRef](#)]
9. Xu, Z.; He, L.; Mu, R.; Zhong, X.; Zhang, Y.; Zhang, J.; Cao, X. Double-ceramic-layer thermal barrier coatings of $\text{La}_2\text{Zr}_2\text{O}_7/\text{YSZ}$ deposited by electron beam-physical vapor deposition. *J. Alloys Compd.* **2009**, *473*, 509–515. [[CrossRef](#)]
10. Guo, S.; Kagawa, Y. Isothermal and cycle properties of EB-PVD yttria-partially-stabilized zirconia thermal barrier coatings at 1150 and 1300 °C. *Ceram. Int.* **2007**, *33*, 373–378. [[CrossRef](#)]
11. Audigié, P.; Put, A.R.-V.; Malié, A.; Thouron, C.; Monceau, D. High-temperature cyclic oxidation of Pt-rich γ - γ' bond-coatings. Part II: Effect of Pt and Al on TBC system lifetime. *Corros. Sci.* **2019**, *150*, 1–8. [[CrossRef](#)]
12. Barjesteh, M.M.; Abbasi, S.M.; Zangeneh Madar, K.; Shirvani, K. Correlation between platinum–aluminide coating features and tensile behavior of nickel-based superalloy Rene® 80. *Rare Met.* **2019**, 1–12. [[CrossRef](#)]
13. Kumawat, M.K.; Sarkar, R.; Jayaram, V.; Alam, M.Z. Fatigue behavior of a freestanding Pt-aluminide (PtAl) bond coat at ambient temperature. *Surf. Coat. Technol.* **2021**, *427*, 127787. [[CrossRef](#)]
14. Lakiza, S.; Hrechanyuk, M.; Red'ko, V.; Ruban, O.; Tyshchenko, J.S.; Makudera, A.; Dudnik, O. The role of hafnium in modern thermal barrier coatings. *Powder Metall. Met. Ceram.* **2021**, *60*, 78–89. [[CrossRef](#)]
15. Texier, D.; Monceau, D.; Selezneff, S.; Longuet, A.; Andrieu, E. High temperature micromechanical behavior of a pt-modified nickel aluminide bond-coating and of its interdiffusion zone with the superalloy substrate. *Metall. Mater. Trans. A* **2020**, *51*, 1475–1480. [[CrossRef](#)]
16. Wang, X.; Zhen, Z.; Huang, G.; Mu, R.; He, L.; Xu, Z. Thermal cycling of EB-PVD TBCs based on YSZ ceramic coat and diffusion aluminide bond coat. *J. Alloys Compd.* **2021**, *873*, 159720. [[CrossRef](#)]
17. Viazzi, C.; Bonino, J.-P.; Ansart, F.; Barnabé, A. Structural study of metastable tetragonal YSZ powders produced via a sol–gel route. *J. Alloys Compd.* **2008**, *452*, 377–383. [[CrossRef](#)]
18. Tsipas, S.A. Effect of dopants on the phase stability of zirconia-based plasma sprayed thermal barrier coatings. *J. Eur. Ceram. Soc.* **2010**, *30*, 61–72. [[CrossRef](#)]
19. Krogstad, J.A.; Lepple, M.; Gao, Y.; Lipkin, D.M.; Levi, C.G.; Green, D.J. Effect of yttria content on the zirconia unit cell parameters. *J. Am. Ceram. Soc.* **2011**, *94*, 4548–4555. [[CrossRef](#)]
20. Borik, M.A.; Bublik, V.T.; Vilkova, M.Y.; Kulebyakin, A.V.; Lomonova, E.E.; Milovich, P.O.; Myzina, V.A.; Ryabockina, P.A.; Tabachkova, N.Y.; Ushakov, S.N. Structure, phase composition and mechanical properties of ZrO_2 partially stabilized with Y_2O_3 . *Mod. Electron. Mater.* **2015**, *1*, 26–31. [[CrossRef](#)]
21. Srinivasan, R.; De Angelis, R.J.; Ice, G.; Davis, B.H. Identification of tetragonal and cubic structures of zirconia using synchrotron X-radiation source. *J. Mater. Res.* **1991**, *6*, 1287–1292. [[CrossRef](#)]
22. Muraleedharan, K.; Subrahmanyam, J.; Bhaduri, S.B. Identification of t' phase in ZrO_2 -7.5 wt% Y_2O_3 Thermal-Barrier Coatings. *J. Am. Ceram. Soc.* **1988**, *71*, C-226–C-227. [[CrossRef](#)]
23. Hajizadeh-Oghaz, M.; Shoja Razavi, R.; Loghman-Estarki, M.R. Synthesis and characterization of non-transformable tetragonal YSZ nanopowder by means of Pechini method for thermal barrier coatings (TBCs) applications. *J. Sol. Gel Sci. Technol.* **2014**, *70*, 6–13. [[CrossRef](#)]
24. Bakan, E.; Vaßen, R. Ceramic top coats of plasma-sprayed thermal barrier coatings: Materials, processes, and properties. *J. Therm. Spray Technol.* **2017**, *26*, 992–1010. [[CrossRef](#)]
25. Dudnik, E.V.; Lakiza, S.N.; Hrechanyuk, I.N.; Ruban, A.K.; Redko, V.P.; Marek, I.O.; Shmibelsky, V.B.; Makudera, A.A.; Hrechanyuk, N.I. Thermal barrier coatings based on ZrO_2 solid solutions. *Powder Metall. Met. Ceram.* **2020**, *59*, 179–200. [[CrossRef](#)]
26. Yang, S. Multiscale modeling of chemo-thermo-mechanical damage of EB-PVD thermal barrier coatings. *J. Mech. Phys. Solids* **2022**, *158*, 104667. [[CrossRef](#)]
27. Shen, Z.; Liu, Z.; Mu, R.; He, L.; Liu, G. Y–Er– ZrO_2 thermal barrier coatings by EB-PVD: Thermal conductivity, thermal shock life and failure mechanism. *Appl. Surf. Sci. Adv.* **2021**, *3*, 100043. [[CrossRef](#)]
28. Vasile, B.S.; Birca, A.C.; Surdu, V.A.; Neacsu, I.A.; Nicoară, A.I. Ceramic composite materials obtained by electron-beam physical vapor deposition used as thermal barriers in the aerospace industry. *Nanomaterials* **2020**, *10*, 370. [[CrossRef](#)]
29. Singh, J.; Quli, F.; Wolfe, D.E.; Schriempf, J.T.; Singh, J. *An Overview: Electron Beam-Physical Vapor Deposition Technology-Present and Future Applications*; Applied Research Laboratory, Pennsylvania State University: University Park, PA, USA, 1999.
30. Suk, O.Y.; Chae, J.-M.; Ryu, H.-I.; Han, Y.; Ahn, J.-K.; Son, M.-S.; Kim, H.-K. Deposition uniformity of 7 wt% YSZ as a thermal barrier coating with different configurational arrangement for turbine blade shape mock-up by electron beam physical vapor deposition. *J. Korean Cryst. Growth Cryst. Technol.* **2019**, *29*, 308–316.
31. Sulaiman, T.A.; Abdulmajeed, A.A.; Donovan, T.E.; Vallittu, P.K.; Narhi, T.O.; Lassila, L.V. The effect of staining and vacuum sintering on optical and mechanical properties of partially and fully stabilized monolithic zirconia. *Dent. Mater. J.* **2015**, *34*, 605–610. [[CrossRef](#)]

32. Borik, M.A.; Chislov, A.S.; Kulebyakin, A.V.; Lomonova, E.E.; Milovich, F.O.; Myzina, V.A.; Ryabochkina, P.A.; Sidorova, N.V.; Tabachkova, N.Y. Effect of heat treatment on the structure and mechanical properties of partially gadolinia-stabilized zirconia crystals. *J. Asian Ceram. Soc.* **2021**, *9*, 559–569. [[CrossRef](#)]
33. Orera, V.M.; Merino, R.I.; Peña, F. $\text{Ce}^{3+} \leftrightarrow \text{Ce}^{4+}$ conversion in ceria-doped zirconia single crystals induced by oxido-reduction treatments. *Solid State Ion.* **1994**, *72*, 224–231. [[CrossRef](#)]
34. Orera, V.M.; Merino, R.I.; Chen, Y.; Cases, R.; Alonso, P.J. Intrinsic electron and hole defects in stabilized zirconia single crystals. *Phys. Rev. B Condens. Matter* **1990**, *42*, 9782–9789. [[CrossRef](#)] [[PubMed](#)]
35. Seok, C.Y.; Gye Won, L.; Woo, J.C.; Sahn, N.; Suk, O.Y. Analysis of phase formation behavior of YSZ-based composites according to rare earth and other oxide doping amounts. *J. Surf. Sci. Eng.* **2022**, *55*, 368–375.

Disclaimer/Publisher’s Note: The statements, opinions and data contained in all publications are solely those of the individual author(s) and contributor(s) and not of MDPI and/or the editor(s). MDPI and/or the editor(s) disclaim responsibility for any injury to people or property resulting from any ideas, methods, instructions or products referred to in the content.